



Mantle transition zone discontinuities beneath the Baikal rift and adjacent areas

Kelly H. Liu^{1,2} and Stephen S. Gao^{1,2}

Received 10 October 2005; revised 13 June 2006; accepted 28 July 2006; published 3 November 2006.

[1] Like most other major continental rifts, the Baikal rift zone (BRZ) in Siberia is presumably underlain by a hot and partially molten mantle, which has a reduced seismic velocity relative to surrounding areas. Recent seismic tomography studies, however, gave conflicting results about the depth extent and even the existence of the low-velocity anomaly beneath the BRZ, suggesting that additional constraints are needed. Here we present results from stacking of about 1700 radial *P*-to-*S* receiver functions from a single long-running seismic station, TLY, located at the SW tip of Lake Baikal. A clear uplift of the 410 km discontinuity (*d*410) with a magnitude of about 47 km relative to the south margin of the Siberian platform is observed beneath the rift. Currently available seismic results suggest that the uplift is unlikely to be caused by addition of water to mantle transition zone (MTZ) silicates but is the result of a 550°C reduction in temperature in the vicinity of the *d*410. In addition, the 660 km discontinuity (*d*660) shows a downward trend toward the rift from the south, suggesting that the entire MTZ might have a low temperature beneath the rift. The thickening of the MTZ suggests a high-velocity anomaly of about 2% in the MTZ, and rules out the possibility that the rifting is caused by a mantle plume originated in or beneath the mantle transition zone.

Citation: Liu, K. H., and S. S. Gao (2006), Mantle transition zone discontinuities beneath the Baikal rift and adjacent areas, *J. Geophys. Res.*, *111*, B11301, doi:10.1029/2005JB004099.

1. Introduction

[2] The Baikal rift zone (BRZ) is the seismically most active rift on earth. On the basis of a seismic catalog compiled by the Advanced National Seismic System (ANSS), a total of eight earthquakes with magnitude 5.5 or larger have occurred inside the rifted valleys during the decade between 1994 and 2003. The rifting was originated along the boundary between the Archean Siberian platform and the Paleozoic-Mesozoic Altai-Sayan-Baikal foldbelt some 35 Myr ago [Logatchev and Zorin, 1992; Keller *et al.*, 1995] (Figure 1). Similar to most other major continental rifts, the BRZ is characterized by higher than normal heat flow [Lysak, 1984], negative gravity anomalies [Zorin *et al.*, 1989], and thinned crust [Zorin *et al.*, 2002; Gao *et al.*, 2004]. Rift-orthogonal mantle flow associated with the rifting and rift-parallel magma-filled cracks beneath the BRZ are suggested by measuring shear wave splitting parameters [Gao *et al.*, 1994a, 1997] and inversion of *P* wave arrival times [Gao *et al.*, 2003]. Surface geologic analyses and focal mechanism studies show that the regional stress in the central area of the BRZ is extensional with a direction of extension orthogonal to the rift axis. In the northern and southern 1/3 of of rift zone, the

regional stress field has a left-lateral strike-slip component [Sherman, 1992].

[3] While most other continental rifts such as the Rio Grande and East African rifts were found to be underlain by a low-velocity zone in the upper mantle and even the mantle transition zone (MTZ, 410–660 km depth range) [e.g., Davis, 1991; Slack *et al.*, 1996; Achauer and Masson, 2002; Wilson *et al.*, 2005a], contradictory seismic tomography results were obtained beneath the BRZ. Most studies suggested low seismic velocities in the upper mantle beneath the rift [e.g., Gao *et al.*, 1994b, 2003; Achauer and Masson, 2002; Friederich, 2003; Brazier and Nyblade, 2003; Tiberi *et al.*, 2003; Zhao *et al.*, 2006], and others did not find such anomalies [e.g., Petit *et al.*, 1998]. The depth extent of the low-velocity anomaly differs greatly among the studies, from less than 100 km to as deep as 600 km. Friederich [2003] suggested a plume-like low-velocity cylindrical anomaly extending from about 135 km to the MTZ, centered at the southern tip of Lake Baikal. Petit *et al.* [1998] suggested a plume-like upwelling of lower mantle material, from a depth of about 700 km to near the surface beneath the southern margin of the Siberian platform. Plume-related origin of continental rifts was also suggested for the East African rift, beneath which a low-velocity structure with a depth extent of about 500 km is found [Ritsema *et al.*, 1998; Nyblade *et al.*, 2000].

[4] While the discrepancies of the tomographic results beneath the BRZ are partially related to the difference in the data sets and techniques used, the intrinsic low resolving power of deep anomalies, especially those in the MTZ, of

¹Department of Geological Sciences and Engineering, University of Missouri-Rolla, Rolla, Missouri, USA.

²Formerly at Department of Geology, Kansas State University, Manhattan, Kansas, USA.

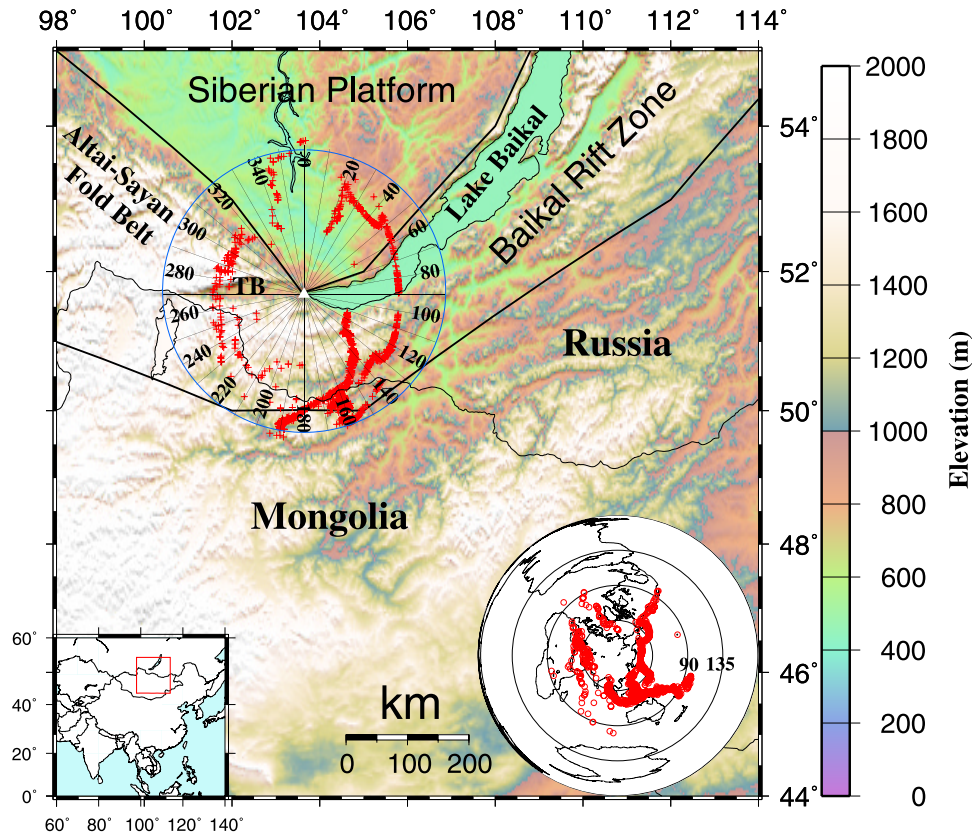


Figure 1. Topographic map of the study area showing tectonic provinces, distribution of ray-piercing points at 540 km depth (crosses), and the azimuthal bins. The bins have a width of 20° and overlap by 10° . Consequently, the central azimuth of the n th bin is $10n$ degrees from the north. Station TLY is represented by the open triangle, and TB is the Tunkin Basin. Tectonically the BRZ is a domal structure in the Altai-Sayan-Baikal foldbelt. In this study we refer the part of the foldbelt west of bin 15 as the Altai-Sayan foldbelt and the eastern part with rifted valleys as the BRZ. The insets show the location of the study area and the epicenters of the earthquakes used in the study, respectively.

all the currently available seismic tomography techniques is perhaps the main cause. Independent constraints of temperature and/or chemical composition anomalies in the MTZ can be provided by measuring spatial variation of the depths of MTZ velocity discontinuities. Under the assumption that variations in the depth of the 410 km discontinuity (d_{410}) and that of the 660 km discontinuity (d_{660}) are thermally induced, numerous studies have inferred temperature variations in the vicinity of the discontinuities [e.g., Dueker and Sheehan, 1998; Shen et al., 2002; Liu et al., 2003]. A 1°C reduction in temperature around d_{410} , which represents the transition from $(\text{Mg,Fe})_2\text{SiO}_4$ (olivine) to its high-pressure polymorph β -spinel (wadsleyite), leads to an uplift of 0.082 km of the d_{410} ; a 1°C reduction in temperature around d_{660} , which represents the phase transition from γ -spinel (ringwoodite) to MgSiO_3 (perovskite) and $(\text{Mg,Fe})\text{O}$ (magnesiowustite), leads to a depression of 0.06 km of the d_{660} . Consequently, a 1 km thickening of the MTZ suggests a uniform temperature reduction of about 7°C [Bina and Helffrich, 1994].

[5] Recently, nonthermal mechanisms for transition zone velocity anomalies and depth variations of d_{410} and d_{660} have gained attention in the geophysical community. One

of such mechanisms is the presence of water in the anhydrous minerals in the MTZ such as wadsleyite and ringwoodite [Wood, 1995; Wood et al., 1996; Smyth and Frost, 2002; Smyth et al., 2006]. Laboratory experiments show that at P,T conditions similar to those near the d_{410} , the depth of the phase transition from olivine to wadsleyite is about 15–40 km shallower for water-saturated peridotite than that for anhydrous peridotite [Smyth and Frost, 2002].

[6] The addition of water can also reduce the P and S wave velocities in the MTZ, and has the potential to broaden the interval of the olivine-wadsleyite phase transition at about 410 km depth, from about 10–20 km in anhydrous minerals, to about 40 km in water-saturated ones [Wood et al., 1996; Smyth and Frost, 2002]. For instance, a transition interval of 20–25 km is expected if the water content in olivine is 500 ppm by weight [Wood, 1995]. This observation was used by van der Meijde et al. [2003] to infer the presence of water brought into the MTZ by past subduction in the vicinity of the d_{410} beneath the Mediterranean region.

[7] Relative to the d_{410} , the effect of water on the depth and transition interval of the d_{660} was not well determined. Most studies suggest that water probably increases the depth of the d_{660} by several km [Higo et al., 2001].

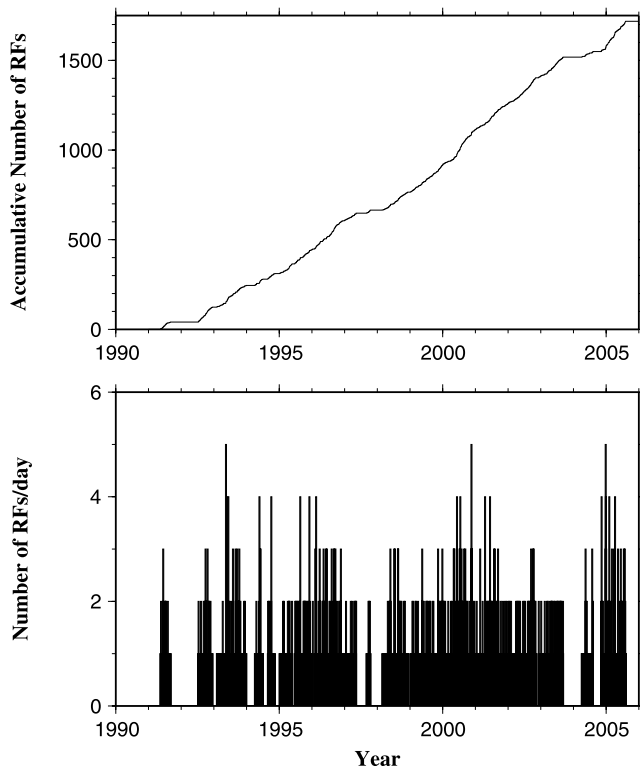


Figure 2. (bottom) Number of high-quality receiver functions per day from station TLY and (top) accumulative number of RFs used in the study.

While some studies have suggested that water increases the interval [Wood *et al.*, 1996], others implied the opposite effect [Higo *et al.*, 2001; van der Meijde *et al.*, 2003].

[8] The present study is aimed at measuring the spatial variation of the depths of d_{410} and d_{660} in the vicinity of the BRZ and the Siberian platform, for the purpose of providing additional constraints on the deep structure, temperature, water content, and dynamics of the rift.

2. Data and Method

[9] The broadband seismograms used in the study were recorded by GSN (Global Seismographic Network) station TLY (Talaya, N51.6807°, E103.6438°, elevation 579 m), managed by IRIS (Incorporated Research Institutions in Seismology). TLY is located on an ancient lake terrace between Lake Baikal and the Tunkin basin [Rogozhin and Yunga, 2000]. The sensors are located about 65 m from the open of a horizontal tunnel in the side of a mountain. The distance between the station and the lake is about 5 km (Figure 1). Tectonically, TLY is situated near the border between the Altai-Sayan fold belt and the Siberian platform [Rogozhin and Yunga, 2000].

[10] High-quality seismic data from TLY have been used in a number of studies. Using Pnl waves from two earthquakes recorded by TLY, Brazier and Nyblade [2003] concluded that the upper mantle beneath the rift axis is 2–5% lower than the surrounding area. Stacking of P -to- S

converted phases recorded by TLY revealed a crustal thickness of 46 km [Gao *et al.*, 2004]. A very narrowband, continuous seismic signal near 2.08 Hz was detected using data from TLY and a portable seismic network over hundreds of km [Liu and Gao, 2001]. Shear wave splitting analysis found a splitting time of 0.82 ± 0.20 s and a fast polarization direction of $129 \pm 4^\circ$, which is approximately parallel to the boundary between the platform and the foldbelt [Gao *et al.*, 1997]. In addition, data from TLY were contributed to a number of seismic tomographic studies of various scales.

[11] For this study, seismograms from teleseismic events (epicentral distance $\Delta = 30^\circ \sim 100^\circ$) occurred between May 1991 and September 2005 were obtained from the IRIS Data Management Center (DMC). The event catalog was compiled by the ANSS. The lower cutoff body wave magnitude is 5.3 for events with Δ between 30° and 75° , and 5.5 for events with Δ between 75° and 100° . The seismograms were band-pass filtered between 0.05 and 0.2 Hz, and manually checked to select those with clear P arrivals on both the vertical and radial components. Radial receiver functions (RFs) were then computed using the procedure of Ammon *et al.* [1990] by deconvolving the radial component with the vertical component, and were screened visually to reject noisy traces. A total of 1718 RFs were used in the study. TLY is one of the earliest stations in GSN and as indicated by the statistics shown in Figure 2, over the past 15 years it has been operating continuously, except for some short interruptions during a few winters.

[12] Both the P -to- S converted phases at the 410 km discontinuity (P_{4S}) and at the 660 km discontinuity (P_{6S}) are clearly observable on the binned receiver functions (Figure 3). P -to- S conversions from the Moho and their multiple reverberations ($PPmS$ and $PSmS$) can also be observed at about 5, 18, and 23 s, respectively, after the direct P wave. A clear arrival around 10 s closely follows the theoretical moveout curve of a discontinuity at the depth of about 90 km, and could be the P -to- S converted phase from the Hales discontinuity observed beneath continents [Green and Hales, 1968; Hales, 1969]. Detailed exploration and discussion of this and other possible discontinuities revealed in the data will be presented elsewhere. Several clusters of arrivals at approximate 30, 40, and 60 s after the P wave do not follow the theoretical moveout curves of P -to- S converted phases well at the corresponding depths, and thus are unlikely to be associated with discontinuities.

[13] We use the RF-stacking approach of Dueker and Sheehan [1998] to enhance the weak P -to- S converted phases originated from the top and bottom discontinuities of the MTZ. To enhance the P -to- S converted phases from a discontinuity at the depth d , the receiver functions are stacked along the moveout curve calculated using

$$T_{P_{dS}} = \int_{-d}^0 \left[\sqrt{V_s(z)^{-2} - p^2} - \sqrt{V_p(z)^{-2} - p^2} \right] dz \quad (1)$$

where p is the ray parameter for the P wave, d is the depth of the candidate discontinuity, and $V_p(z)$ and $V_s(z)$ are the P and S wave velocities, respectively, at depth z . The

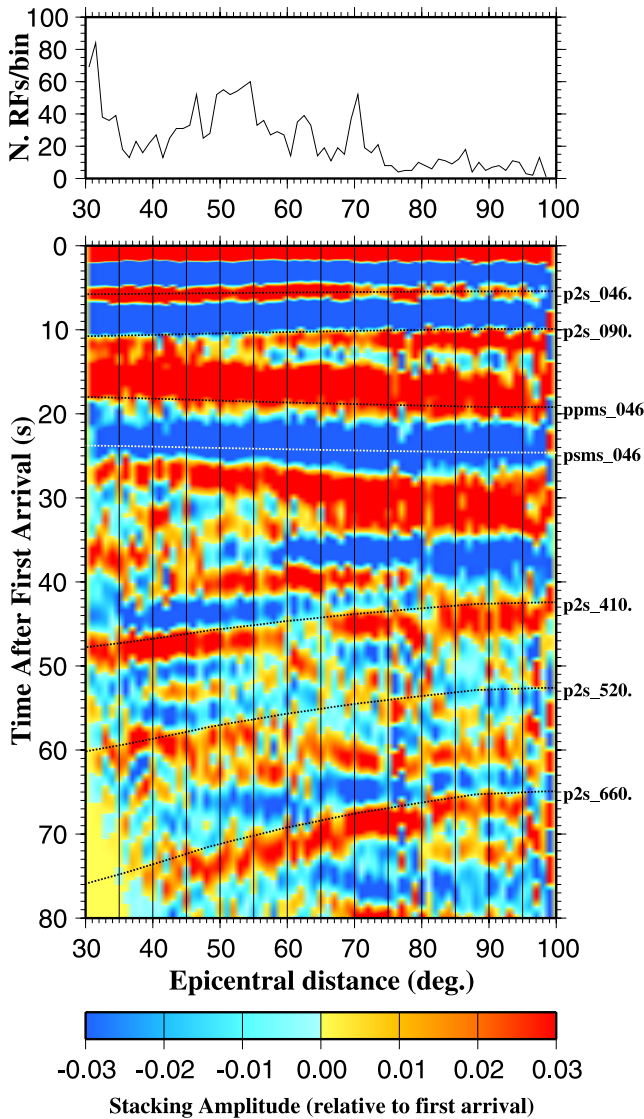


Figure 3. (bottom) Stacked radial receiver functions. The 1718 radial receiver functions used in the study are arranged according to their depth-corrected epicentral distances into 1° ranges and those in the same range are then stacked. The dashed lines labeled as P2S_xyz are predicted moveout curves for P -to- S converted phases at depth xyz km, and the lines labeled as PPmS_046 and psms_046 are the Moho (which has a depth of 46 km) reverberation phases, PPmS and PSmS, respectively. (top) Number of receiver functions per bin.

receiver functions, which are time series, are then stacked and converted to depth series using

$$A(d) = \frac{1}{N} \sum_{i=1}^N A_i(T_{PdS}^{(i)}) \quad (2)$$

where $A(d)$ is the stacking amplitude for a candidate discontinuity at depth d , N is the number of traces (i.e., the number of ray-piercing points of qualified receiver functions at depth d), $T_{PdS}^{(i)}$ is the P_dS moveout time of

the i th receiver function for a discontinuity computed using equation (1), and $A_i(T_{PdS}^{(i)})$ is the amplitude of the i th receiver function at time $T_{PdS}^{(i)}$. In equation (2) the reference time for each trace is the time of the first P arrival. The candidate depths have an increment of 1 km, and range from 200 to 800 km. The IASP91 Earth model [Kennett and Engdahl, 1991] is used to calculate the coordinates of the ray-piercing points of the P -to- S converted phases and the moveout times. As discussed in section 4.1, while the use of a standard earth model could lead to errors of up to a few kilometers in the resulting depths of the MTZ discontinuities, it has insignificant effect on the main conclusions of the study.

[14] The RFs were grouped based on the backazimuths of the events relative to the station, and the locations of the piercing points at 540 km, which is approximately the center of the MTZ, are shown in Figure 1. The piercing points are distributed along the periphery of an approximately circular area, with a total length of about 1000 km. Given the approximately circular distribution of the piercing points, we grouped them into azimuthal bins of 20° centered at the station (Figure 1). Receiver functions with piercing points in the same bins were stacked using the procedure above. We used a 10° overlap between adjacent bins to ensure a sufficient number of stackings. The bins are numbered according to $(\phi_1 + \phi_2)/20$, where ϕ_1 and ϕ_2 are the lower and upper limits of the azimuthal bins, respectively. We tested the robustness of the resulting anomalies by varying the bin size, and by using nonoverlapping bins, and found that similar results were obtained if the bin size is 10° or larger.

[15] The bootstrap resampling procedure [Press et al., 1992; Efron and Tibshirani, 1986] was used to estimate the standard deviations (STDs) of the discontinuity depths. For each bootstrap step, we randomly choose $1-1/e = 63\%$ independent receiver functions from the original data set. About 60% of the chosen ones were then duplicated so that the total number of the new set of receiver functions is the same as that of the original set. The new set of receiver functions were then stacked to produce images of discontinuities. The resulting depth of a particular discontinuity is expected to be distributed around the true depth [Press et al., 1992], and the STD is calculated using

$$\sigma = \sqrt{\frac{1}{M-1} \sum_{i=1}^M (D_i - \bar{D})^2},$$

where M is the number of bootstrap steps (which is taken as 20 in the study), D_i is the resulting depth of the i th step, and \bar{D} is the mean depth. The STDs of the MTZ thickness, σ_d , is calculated using $\sqrt{\sigma_4^2 + \sigma_6^2}$, where σ_4 and σ_6 is the STD of $d410$ and $d660$, respectively.

3. Results

[16] On the basis of previous observations of the possible depth variation of $d410$ and $d660$ and the characteristics of our resulting phasing depth images (Figure 4), we consider the largest positive arrival in the depth range of 380–450 km as $P4S$, and that in the depth range of 660–720 km as $P6S$. The results are summarized in Table 1. About 80% of the

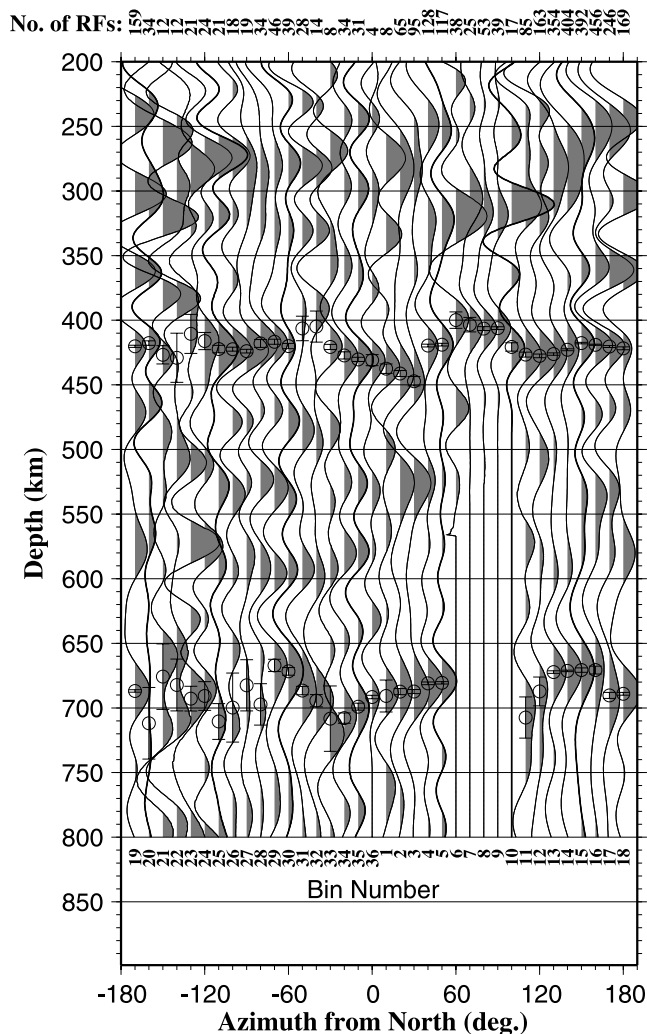


Figure 4. Results from stacking of radial receiver functions beneath the azimuthal bins. Positive polarities of the traces are shaded. The traces were normalized by the average of the maximum amplitudes in the 400–450 and 660–720 depth ranges. The number of receiver functions per bin at 540 km depth are show at the top. Mean depths and their STDs from the bootstrap steps are shown as circles and bars in the 400–450 and 650–700 km depth ranges.

ray-piercing points are distributed on the eastern half (bins 2–19) of the study area (Figure 1), suggesting that the discontinuities beneath the eastern half were better determined than those beneath the western half. The low resolving power on the western half is reflected by the large STDs (Figure 5). Consequently, discussions below will be concentrated on the eastern half, where the BRZ is located.

3.1. The 410 km Discontinuity (d_{410})

[17] The depth to d_{410} varies from 400 ± 6 km beneath bin 6 to 447 ± 4 km beneath bin 3. The mean depth is 421 ± 2 km, which is slightly deeper than the global average of 418 km [Flanagan and Shearer, 1998].

[18] Beneath the Altai-Sayan fold belt (approximately from bins 15 to 31), d_{410} is relatively flat with a depth that

is close to the mean (Figure 6). A significant deepening of d_{410} toward the rift axis with a magnitude of about 25 km is observed beneath the Siberia platform (bins 33–3), corresponding to an increase in mantle temperature of about 300°C in the vicinity of the d_{410} .

[19] An uplift of the d_{410} is found between bins 3 and 11 with a magnitude of 47 km. The uplift is centered at bin 7, which is beneath the lake (Figure 6). Under the assumption that the uplift has a thermal origin, the magnitude of the uplift suggests a temperature reduction of about 550°C beneath the rift relative to the south margin of the platform.

3.2. The 660 km Discontinuity (d_{660})

[20] The d_{660} beneath bins 6 and 10 cannot be imaged, due to the fact that P waves from earthquakes in the back-azimuthal range of $50^\circ \sim 110^\circ$ (western Pacific subduction zone) are too close to traverse d_{660} . The mean depth of d_{660} (688 ± 2 km) is significantly greater than the global average of 660 km [Flanagan and Shearer, 1998].

[21] An uplift of the d_{660} between bins 25 and 33 is observed beneath the foldbelt, centered near the Tunkin Basin (Figure 6). The southern half of the uplift, however, cannot be well-determined due to the small number of RFs and resulting large STDs. If the uplift can be confirmed using additional data, it could suggest a thermal anomaly with a lateral temperature contrast of several hundred degrees at the bottom of the MTZ. A possible cause of the anomaly is a mantle plume that has not reached the d_{410} .

[22] Beneath the platform, d_{660} shallows gradually toward the rift, from 708 km beneath bin 34 to 681 km beneath bin 5, corresponding to a temperature increase of about 460° . South of the lake, the two bins (11 and 12) that are closest to the lake suggest a rapid increase in the depth of d_{660} , in spite of the large STDs.

3.3. MTZ Thickness

[23] The global averages for the depths of the d_{410} and d_{660} are 418 and 660 km, respectively [Flanagan and Shearer, 1998], resulting in a MTZ thickness of 242 km. The thickness of the MTZ in our study area ranges from 240 to 293 km, with a mean of 264 ± 3 km, suggesting a colder MTZ on average. This is consistent with a previous global-scale study using SS precursors, which shows a thickened MTZ beneath central and eastern Siberia [Flanagan and Shearer, 1998].

[24] The MTZ beneath the platform thickens gradually toward the interior of the platform, from 240 km (which is close to the global average) beneath bin 3, to 290 km beneath bin 32 (Figure 6). This corresponds to a decrease in temperature of about 380°C . The variations of d_{410} and d_{660} contribute to the thickening of the MTZ approximately equally, suggesting that the temperature of the entire MTZ decreases toward the interior of the platform. The trend is similar to what was observed across the Kaapvaal craton in southern Africa [Gao *et al.*, 2002]. The area south of the lake, bins 13–16, also shows a MTZ thickness that is close to the global average.

[25] Beneath the lake, the depth extent of the thickened region (relative to the platform) suggested by the uplifted d_{410} cannot be accurately determined due to the lack of seismic rays that traverse d_{660} beneath bins 6–10. If we

Table 1. Resulting Depths of $d410$ and $d660$ and MTZ Thickness H

Bin	Azimuth Range, deg	$d410$, km	σ_{d410} , km	$d660$, km	σ_{d660} , km	H , km	σ_H , km	N
1	0–20	437.50	3.66	690.75	12.36	253.25	12.89	8
2	10–30	441.25	2.31	687.35	2.37	246.10	3.31	65
3	20–40	447.20	3.64	687.30	1.56	240.10	3.96	95
4	30–50	419.60	1.05	680.95	1.05	261.35	1.48	128
5	40–60	418.90	1.07	680.55	0.94	261.65	1.42	117
6	50–70	399.90	6.37	—	—	—	—	30
7	60–80	403.45	5.61	—	—	—	—	1
8	70–90	406.45	1.47	—	—	—	—	0
9	80–100	406.10	1.07	—	—	—	—	0
10	90–110	420.65	3.25	—	—	—	—	0
11	100–120	426.60	1.88	707.40	15.96	280.80	16.07	26
12	110–130	427.60	1.43	687.25	11.15	259.65	11.24	102
13	120–140	426.15	0.93	672.25	0.97	246.10	1.34	329
14	130–150	422.85	0.75	671.35	0.59	248.50	0.95	389
15	140–160	417.70	0.57	670.70	1.69	253.00	1.78	325
16	150–170	419.00	0.46	670.70	3.01	251.70	3.04	409
17	160–180	420.35	0.75	690.30	2.36	269.95	2.48	244
18	170–190	421.75	1.12	689.05	1.10	267.30	1.57	169
19	180–200	420.20	0.83	686.85	0.99	266.65	1.29	159
20	190–210	417.70	1.72	711.85	27.70	294.15	27.75	34
21	200–220	426.75	7.06	675.75	25.35	249.00	26.31	12
22	210–230	429.05	19.00	682.20	20.05	253.15	27.62	12
23	220–240	410.55	15.10	692.80	9.59	282.25	17.89	19
24	230–250	416.10	6.66	690.75	11.11	274.65	12.95	23
25	240–260	422.30	2.89	710.45	13.85	288.15	14.15	21
26	250–270	422.40	1.57	699.70	26.71	277.30	26.76	18
27	260–280	423.90	1.41	682.45	19.79	258.55	19.84	19
28	270–290	417.95	3.03	697.25	15.99	279.30	16.27	34
29	280–300	416.65	1.95	667.10	4.72	250.45	5.11	46
30	290–310	420.00	2.05	671.70	2.94	251.70	3.58	39
31	300–320	406.40	9.49	686.55	3.24	280.15	10.03	28
32	310–330	404.90	12.01	694.40	4.75	289.50	12.92	14
33	320–340	420.70	2.00	708.25	25.31	287.55	25.39	8
34	330–350	427.25	2.79	707.85	3.98	280.60	4.86	34
35	340–360	430.30	1.59	699.00	2.68	268.70	3.12	31
36	350–370	430.90	4.27	691.55	1.32	260.65	4.47	4

assume that the lateral temperature anomaly in the entire MTZ is uniformly -550°C (which is suggested by the magnitude of the uplift of $d410$), an approximately 30 km depression of the $d660$ is expected. This is comparable with the magnitude of the deepening of the $d660$ beneath bins 11 and 12. Under the assumption that $\partial V_p / \partial T = -4.1 \times 10^{-4} \text{ km/s}^\circ\text{C}$ [Anderson, 1989], the increase in P wave velocity is about 0.2 km/s, corresponding to a 2% high-velocity anomaly in the MTZ. The observed variation of the MTZ thickness is consistent with seismic tomography results. Although most seismic tomography studies [e.g., Achauer and Masson, 2002; Gao et al., 1994b, 2003; Tiberi et al., 2003] revealed low-velocity regions in the upper mantle beneath the rift, there still lacks strong evidence for such anomalies extending to the MTZ. On the contrary, a recent seismic tomography study [Zhao et al., 2006] suggested a high-velocity region with a magnitude of 1–2% in the MTZ beneath the rift.

4. Discussion and Conclusions

4.1. Errors Due to the Use of a Standard Earth Model

[26] The IASP91 Earth model [Kennett and Engdahl, 1991] is used as $V_p(z)$ and $V_s(z)$ in equation (1) for moveout corrections. This leads to an error in the apparent depth of a discontinuity if the velocities above it is different from the IASP91 model. However, we estimated that the use of a realistic, 3D velocity model will lead to a change of the

depth to the $d410$ or $d660$ of only a few km, which is much smaller than the magnitude of the anomalies discussed below. It has even less significant effects on the transition zone thickness because the similarity in the raypath of $P4S$ and $P6S$. In addition, if a model with a lower upper mantle velocity beneath the BRZ is used, which is expected for a rift and was suggested by most tomography studies, the resulting magnitude of the uplift of the $d410$ would actually increase by a couple of km. It would also increase by a few km if the effect of high attenuation in the upper mantle [Gao et al., 1994b] is corrected, as suggested by a recent synthetic study [Liu, 2003].

[27] Velocity heterogeneities in the MTZ do have an effect on the depth of $d660$. Under the assumption that the MTZ beneath the BRZ has an uniformly high velocity anomaly of 2%, the depth of resulting $d660$ is over estimated by about 5 km due to the use of the IASP91 model. This is several times smaller than the observed lateral variation of the depth to $d660$.

[28] Under some circumstances, velocity anisotropy could also lead to apparent topography variations in the resulting images. In the area covered by the piercing points (Figure 1), our previous studies [Gao et al., 1994a, 1997] revealed that the fast polarization directions (ϕ) of split shear waves vary spatially and most of them have a rift-parallel component. The time delays between the fast and slow components are in the order of 1 s, and is most likely

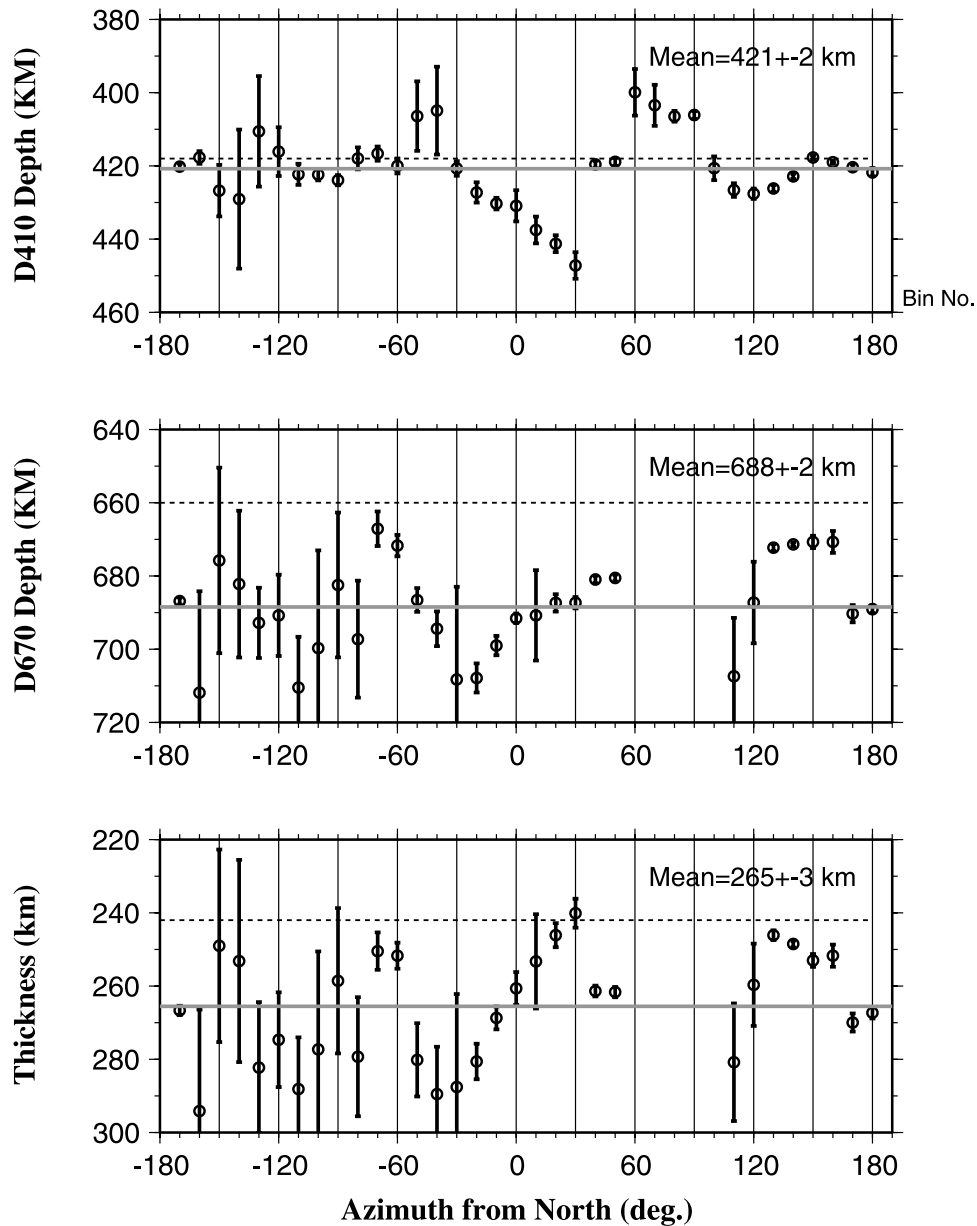


Figure 5. Resulting discontinuity depths and mantle transition zone thickness. The gray horizontal lines show the averages from this study, and the dashed lines show global averages [Flanagan and Shearer, 1998].

originated from the upper mantle [Gao *et al.*, 1994a, 1997], suggesting that for radial RFs from earthquakes with a backazimuth that is close to ϕ or $\phi \pm 180^\circ$, the P -to- S converted phase will arrive about 1 s earlier than those from a direction that is orthogonal to ϕ . This would affect both transition zone discontinuities and lead to an apparent depth of about 5 km shallower for events from the former azimuthal group relative to the other group. Because the magnitude of the observed transition zone topography is several times larger than 5 km, the possibility that the observed transition zone topography is due to seismic anisotropy can be ruled out.

[29] Thus the use of a standard earth model in calculating the moveout times and the location of the ray-piercing points has insignificant effects on the main conclusions of

the study, i.e., the BRZ is underlain by a thickened MTZ, as most clearly suggested by the uplift of the $d410$. In addition, the currently available velocity models for the study area [e.g., Zhao *et al.*, 2006; Gao *et al.*, 2003; Tiberi *et al.*, 2003; Achauer and Masson, 2002; Petit *et al.*, 1998] show considerable inconsistencies with each other. This will make it difficult technically to use any one of them for the correction.

4.2. On the Use of Data From a Single Station

[30] This study is somewhat unconventional in that it uses data from a single, long-running seismic station. TLY is among the earliest GSN stations and is perhaps one of the small number of stations with the least amount of interruptions in operation (Figure 2). Consequently, the number

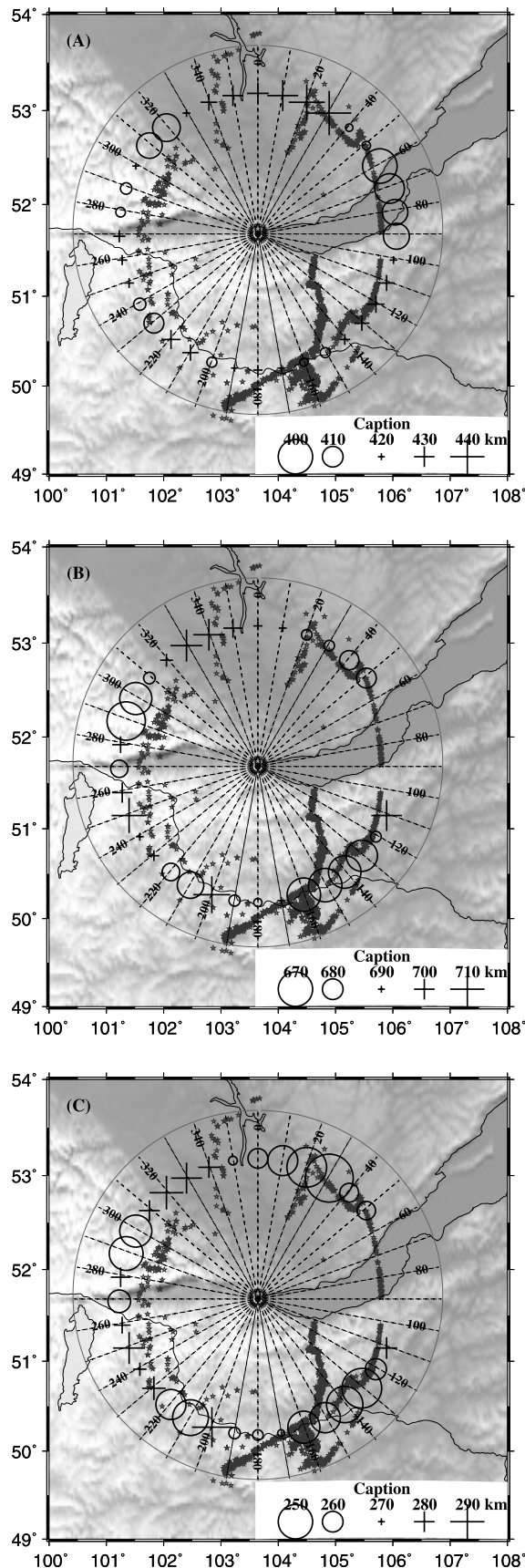


Figure 6. Resulting (a) depth to d_{410} ; (b) depth to d_{660} ; and (c) MTZ thickness for each of the azimuthal bins. Gray stars are ray-piercing points at 540 km depth.

of available high-quality RFs [1718] is comparable or even more than most previous studies of MTZ discontinuities using data from portable experiments. For instance, the number of RFs from the Rocky Mountain Front experiment is 365 [Dueker and Sheehan, 1998], that from the large-scale southern African Seismic Experiment is about 1500 [Gao *et al.*, 2002], and that from the combined data set from three portable experiments conducted across central South America is about 2100 [Liu *et al.*, 2003]. Therefore, as long as the number of high-quality RFs is sufficient for imaging the targeted discontinuities beneath areas of interest, using of data from a single station has no clear disadvantages.

[31] Compared with data sets from a multistation network, the use of a uniform data set from a long-running single station has several differences. First, because the rays are distributed in a cone centered at the station, the area traveled by the rays is smaller in the crust and uppermost mantle, where strong spatial variation in seismic velocities is common. Consequently, effects of near-surface heterogeneities on the resulting depths of d_{410} and d_{660} are smaller. For instance, the ray-piercing points at the Moho spread an approximately circular area with a radius of about 10 km, within which variation in crustal thickness/velocity is expected to be less significant than that over a larger area covered by a multistation network.

[32] Second, the frequency response of all the seismograms is likely to be the same (under the assumption of insignificant temporal variation within the instrument), resulting in more coherent stacking.

[33] Third, because of the similarity in crustal and upper mantle structures and in surface topographic features, signal-generated noises and reverberations could be more similar over the events. This similarity might lead to more coherent stacking of the noises and reverberations, and result in false discontinuities. However, because the RFs are stacked along the moveout curves of the P_dS phases, non- P_dS arrivals such as noise and reverberations are compressed. Additionally, P_4S and P_6S which are the targets of the present study, are robust and follow the theoretical moveout curves well (Figure 3). Therefore signal-generated noises and reverberations are unlikely to affect the resulting images.

4.3. Possible Causes of the MTZ Discontinuity Topography

[34] The most commonly used interpretation for significant uplift of the d_{410} and depression of the d_{660} is the reduced temperature related to a subducted slab [e.g., Shearer and Masters, 1992; Flanagan and Shearer, 1998; Liu *et al.*, 2003]. If this is the case, our observations (Figure 5) suggests that the thickening of the MTZ associated with the slab could be as large as 90 km, which corresponds to a reduction of about 650°C in MTZ temperature.

[35] However, in spite of the attractiveness and simplicity of the model, several counterarguments suggest that it is unrealistic. First, the lack of mantle earthquakes and any GPS-revealed plate convergence in the area [Calais *et al.*, 1998] suggests that the slab, if exists, has become inactive and thus must be a slab associated with past subduction. Second, the thickening of the MTZ related to the assumed inactive slab is too large, even when compared with active subduction zones. For instance, our previous study [Liu *et*

al., 2003] across central South America using the same receiver function procedure as the one used here found a thickening of about 50 km associated with the Nazca slab, which is about half of the observed value associated with the assumed inactive subducted slab beneath BRZ. Third, none of the seismic tomography studies suggested the existence of such a slab. Therefore the observed spatial variations of the mantle discontinuity topography is unlikely caused by a subducted slab in the MTZ.

[36] The second possible mechanism that can lead to the observed depth variations of the MTZ discontinuities is the presence of water in wadsleyite (for $d410$) and ringwoodite (for $d660$) [Wood *et al.*, 1996; Smyth and Frost, 2002]. Because the configuration of the global seismicity does not allow us to obtain a well-imaged $d660$ beneath the BRZ, and also because the effect of water on the sharpness and topography of the $d660$ is not well understood, in the following the discussion will be focused on the effect of H₂O on the $d410$.

[37] As suggested by laboratory experiments [e.g., Smyth and Frost, 2002], a larger water content in wadsleyite leads to a greater uplift of the $d410$ and lower MTZ seismic velocities. If there is vertical mantle flow traveling across the $d410$, the Water also tends to reduce the sharpness of the $d410$ [Wood, 1995; van der Meijde *et al.*, 2003].

[38] Under this model, the uplift of the $d410$ beneath the rift axis is related to an excessive (relative to the surrounding area) amount of water in the top of the MTZ. However, results from previous seismic tomography studies and those presented here are not consistent with this model. Similar to most previous work, a recent teleseismic P wave tomography study [see Zhao *et al.*, 2006, Figure 5d] did not reveal a low-velocity area beneath the BRZ in the region of the MTZ sampled by the P -to- S converted phases. Instead, a high-velocity area with a magnitude of 1–2% was revealed almost exactly beneath the area with uplifted $d410$. Check-board tests suggest that the high-velocity anomaly was well resolved [Zhao *et al.*, 2006]. Because water is expected to decrease the velocities, the lack of a low velocity zone in the top part of the MTZ suggests that relative to the surrounding area, the top part of the MTZ directly beneath the BRZ does not contain more hydrous minerals.

[39] In addition, if excessive amount of water is the cause of the observed $d410$ uplift, the pulse width of the $P4S$ is expected to increase, and their amplitudes are expected to decrease in the area with the uplifted $d410$ relative to the surrounding area [van der Meijde *et al.*, 2003]. On the basis of the observations that there is no clear reduction in amplitude or the broadening of the pulses of $P4S$ (Figure 4), we conclude that the model that excessive water is the major cause of the observed uplift of $d410$ is not plausible. Additionally, there is no simple explanation about how more water could concentrate beneath the BRZ than the surrounding areas.

[40] The third possible mechanism for the observed transition zone discontinuity topography is the thermal anomalies possibly associated with rifting process. Beneath the Tanzania craton and the eastern branch of the East African rift, a receiver function study [Owens *et al.*, 2000] revealed a depression of the $d410$, which, together with the existence of a low-velocity zone to the depth of at least 500 km [Ritsema *et al.*, 1998], led to the suggestion of a hotter MTZ. A mantle

plume originated from beneath the $d410$ is suggested to explain the seismic results [Nyblade *et al.*, 2000]. Beneath the Rio Grande Rift, however, both $d410$ and $d660$ are found to be relatively flat [Wilson *et al.*, 2005b], suggesting a MTZ that is normal in terms of temperature. The observed uplift of $d410$ and possible depression of the $d660$ beneath the BRZ suggest a MTZ that is colder than the surrounding areas.

[41] The uplift of $d410$ rules out the possibility that the rifting is due to a mantle plume originated below $d410$. Our results are thus inconsistent with some of the tomographic studies [e.g., Petit *et al.*, 1998; Friederich, 2003] which suggested a plume-related rifting process. However, the possibility that the rifting is related to a plume originated in the upper mantle cannot be excluded based on existing data. To our knowledge, this is the first time that a cold MTZ is suggested beneath a major continental rift, and so far no existing geodynamic or mineralogic models can explain the unexpected result. One possible cause of the low temperature in the MTZ is that the opening of the rift at about 35 Myr ago has created a zone of high surface heat flux [Lysak, 1984] and partial melt (and consequently reduction in seismic velocity) in the upper mantle beneath the rift. Under the assumption that the amount of heat generation is similar beneath the entire area of study, the high surface heat flux in the rift could lead to reduced temperature of the upper mantle and MTZ. This model, however, remains quite speculative until additional information regarding the thermal history and thermal properties beneath the study area can be obtained so that vigorous geodynamic modeling can be performed.

[42] In summary, using data from a single broadband station, we have imaged spatial variation of mantle transition zone discontinuities. The main features are the unexpected uplift of the $d410$ and possible depression of $d660$, suggesting a reduced temperature and increased velocity with a magnitude of 2% in the mantle transition zone beneath the BRZ relative to the southern margin of the Siberian platform. We also observed a gradual cooling of the MTZ beneath the Siberian platform toward its interior. Finally, this study demonstrated the effectiveness of data from a single, long-running, high-quality seismic station in the study of the structure and dynamics of the deep interior of the Earth.

[43] **Acknowledgments.** Data used in the study were archived and managed by the IRIS DMC. Special thanks are given to Mary Edmunds and Anh Ngo. Constructive reviews by Matt Fouch and Hersh Gilbert and discussions with Dapeng Zhao significantly improved the manuscript. We thank Joe Smyth for discussions on the possible effects of water on mantle transition zone discontinuities. The study was supported by the National Science Foundation under awards EAR-0207466 and EAR-0440320.

References

- Achauer, U., and F. Masson (2002), Seismic tomography of continental rifts revisited: from relative to absolute heterogeneities, *Tectonophysics*, 358, 17–37.
- Ammon, C. J., G. E. Randall, and G. Zandt (1990), On the non-uniqueness of receiver function inversions, *J. Geophys. Res.*, 95, 15,303–15,318.
- Anderson, D. L. (1989), *Theory of the Earth*, Blackwell Sci., Malden, Mass.
- Bina, C. R., and G. Helffrich (1994), Phase transition Clapeyron slopes and transition zone seismic discontinuity topography, *J. Geophys. Res.*, 99, 15,853–15,860.
- Brazier, R. A., and A. A. Nyblade (2003), Upper mantle P velocity structure beneath the Baikal Rift from modeling regional seismic data, *Geophys. Res. Lett.*, 30(4), 1153, doi:10.1029/2002GL016115.
- Calais, E., O. Lesne, J. Deverchere, V. A. Sankov, A. V. Likhnev, A. I. Miroshnichenko, and K. G. Levi (1998), Crustal deformation in the Baikal rift from GPS measurements, *Geophys. Res. Lett.*, 25, 4003–4006.

- Davis, P. M. (1991), Continental rift structures and dynamics with reference to teleseismic studies of the Rio Grande and East African rifts, *Tectonophysics*, *197*, 309–325.
- Dueker, K. G., and A. F. Sheehan (1998), Mantle discontinuity structure beneath the Colorado Rocky Mountains and High Plains, *J. Geophys. Res.*, *103*, 7153–7169.
- Efron, B., and R. Tibshirani (1986), Bootstrap methods for standard errors, confidence intervals, and other measures of statistical accuracy, *Stat. Sci.*, *1*, 54–75.
- Flanagan, M. P., and P. M. Shearer (1998), Global mapping of topography on transition zone velocity discontinuities by stacking *SS* precursors, *J. Geophys. Res.*, *103*, 2673–2692.
- Friederich, W. (2003), The *S*-velocity structure of the east Asian mantle from inversion of shear and surface waveforms, *Geophys. J. Int.*, *153*, 88–102.
- Gao, S., P. M. Davis, H. Liu, P. D. Slack, Y. A. Zorin, V. V. Mordvinova, V. M. Kozhevnikov, and R. P. Meyer (1994a), Seismic anisotropy and mantle flow beneath the Baikal rift Zone, *Nature*, *371*, 149–151.
- Gao, S., P. M. Davis, H. Liu, P. Slack, Y. A. Zorin, N. A. Logatchev, M. Kogan, P. Burkholder, and R. P. Meyer (1994b), Asymmetric upwarp of the asthenosphere beneath the Baikal rift zone, Siberia, *J. Geophys. Res.*, *99*, 15,319–15,330.
- Gao, S., P. M. Davis, H. Liu, P. D. Slack, A. W. Rigor, Y. A. Zorin, V. V. Mordvinova, V. M. Kozhevnikov, and N. A. Logatchev (1997), *SKS* splitting beneath continental rift zones, *J. Geophys. Res.*, *102*, 22,781–22,797.
- Gao, S. S., P. G. Silver, K. H. Liu, and Kaapvaal Seismic Group (2002), Mantle discontinuities beneath southern Africa, *Geophys. Res. Lett.*, *29*(10), 1491, doi:10.1029/2001GL013834.
- Gao, S. S., K. H. Liu, P. M. Davis, P. D. Slack, Y. A. Zorin, V. V. Mordvinova, and V. M. Kozhevnikov (2003), Evidence for small-scale mantle convection in the upper mantle beneath the Baikal rift zone, *J. Geophys. Res.*, *108*(B4), 2194, doi:10.1029/2002JB002039.
- Gao, S. S., K. H. Liu, and C. Chen (2004), Significant crustal thinning beneath the Baikal rift zone: New constraints from receiver function analysis, *Geophys. Res. Lett.*, *31*, L20610, doi:10.1029/2004GL020813.
- Green, R. W. E., and A. L. Hales (1968), The travel times of *P* waves to 30° in the central United States and upper mantle structure, *Bull. Seismol. Soc. Am.*, *58*, 267–289.
- Hales, A. L. (1969), A seismic discontinuity in the lithosphere, *Earth Planet. Sci. Lett.*, *7*, 44–46.
- Higo, Y., T. Inoue, T. Irfune, and H. Yurimoto (2001), Effect of water on the spinel-postspinel transformation in Mg_2SiO_4 , *Geophys. Res. Lett.*, *28*(18), 3505–3508.
- Keller, G. R., M. Bott, R. F. Wendlandt, D. I. Doser, and P. Morgan (1995), The Baikal rift system, in *Continental Rifts: Evolution, Structure, Tectonics*, Elsevier, New York.
- Kennett, B. L. N., and E. R. Engdahl (1991), Traveltimes for global earthquake location and phase identification, *Geophys. J. Int.*, *105*, 429–465.
- Liu, K. H. (2003), Effects of inelasticity on the apparent depth and detectability of seismic discontinuities in the mantle, *Geophys. Res. Lett.*, *30*(9), 1455, doi:10.1029/2002GL015264.
- Liu, K. H., and S. S. Gao (2001), Characterization of a continuous, very narrowband seismic signal near 2.08 Hz, *Bull. Seismol. Soc. Am.*, *91*, 1910–1916.
- Liu, K. H., S. S. Gao, P. G. Silver, and Y. Zhang (2003), Mantle layering across central South America, *J. Geophys. Res.*, *108*(B11), 2510, doi:10.1029/2002JB002208.
- Logatchev, N. A., and Y. A. Zorin (1992), Baikal rift zone—Structure and geodynamics, *Tectonophysics*, *208*, 273–286.
- Lysak, S. V. (1984), Terrestrial heat flow in the south of east Siberia, *Tectonophysics*, *103*, 205–215.
- Nyblade, A. A., T. J. Owens, H. Gurrola, J. Ritsema, and C. A. Langston (2000), Seismic evidence for a deep upper mantle thermal anomaly beneath east Africa, *Geology*, *28*, 599–602.
- Owens, T. J., A. A. Nyblade, H. Gurrola, and C. A. Langston (2000), Mantle transition zone structure beneath Tanzania, east Africa, *Geophys. Res. Lett.*, *27*, 827–830.
- Petit, C., I. Koulakov, and J. Deverchere (1998), Velocity structure around the Baikal rift zone from teleseismic and local earthquake travel-times and geodynamic implications, *Tectonophysics*, *296*, 125–144.
- Press, W. H., S. A. Teukolsky, W. T. Vetterling, and B. P. Flannery (1992), *Numerical recipes in FORTRAN*, 2nd ed., Cambridge Univ. Press, New York.
- Ritsema, J., A. A. Nyblade, T. J. Owens, C. A. Langston, and J. C. VanDecar (1998), Upper mantle seismic velocity structure beneath Tanzania, east Africa: Implications for the stability of cratonic lithosphere, *J. Geophys. Res.*, *103*, 21,201–21,213.
- Rogozhin, E. A., and S. L. Yunga (2000), *The Geological and Geophysical Environment at Russian IRIS GSN Stations*, edited by K. Fujita, IRIS Consortium, New York.
- Shearer, P. M., and T. G. Masters (1992), Global mapping of topography on the 660-km discontinuity, *Nature*, *355*, 791–796.
- Shen, Y., S. C. Solomon, I. Th. Bjarnason, G. Nolet, W. J. Morgan, R. M. Allen, K. Vogfjord, S. Jakobsdottir, R. Stefansson, B. R. Julian, and G. R. Foulger (2002), Seismic evidence for a tilted mantle plume and north-south mantle flow beneath Iceland, *Earth Planet. Sci. Lett.*, *197*, 261–272.
- Sherman, S. I. (1992), Faults and tectonic stresses of the Baikal rift zone, *Tectonophysics*, *208*, 297–307.
- Slack, P. D., P. M. Davis, W. S. Baldrige, K. H. Olsen, A. Glahn, U. Achauer, and W. Spence (1996), The upper mantle structure of the central Rio Grande Rift region from teleseismic *P* and *S* wave travel time delays and attenuation, *J. Geophys. Res.*, *101*, 16,003–16,023.
- Smyth, J. R., and D. J. Frost (2002), The effect of water on the 410-km discontinuity: An experimental study, *Geophys. Res. Lett.*, *29*(10), 1485, doi:10.1029/2001GL014418.
- Smyth, J. R., D. J. Frost, F. Nestola, C. M. Holl, and G. Bromiley (2006), Olivine hydration in the deep upper mantle: Effects of temperature and silica activity, *Geophys. Res. Lett.*, *33*, L15301, doi:10.1029/2006GL026194.
- Tiberi, C., M. Diament, J. Déverchère, C. Petit-Mariani, V. Mikhailov, S. Tikhotsky, and U. Achauer (2003), Deep structure of the Baikal rift zone revealed by joint inversion of gravity and seismology, *J. Geophys. Res.*, *108*(B3), 2133, doi:10.1029/2002JB001880.
- van der Meijde, M., F. Marone, D. Giardini, and S. van der Lee (2003), Seismic evidence for water deep in Earth's upper mantle, *Science*, *300*, 1556–1558.
- Wilson, D., R. Aster, M. West, J. Ni, S. Grand, W. Gao, W. S. Baldrige, S. Semken, and P. Patel (2005a), Lithospheric structure of the Rio Grande Rift, *Nature*, *433*, 851–855.
- Wilson, D., R. Aster, J. Ni, S. Grand, M. West, W. Gao, W. S. Baldrige, and S. Semken (2005b), Imaging the seismic structure of the crust and upper mantle beneath the Great Plains, Rio Grande Rift, and Colorado Plateau using receiver functions, *J. Geophys. Res.*, *110*, B05306, doi:10.1029/2004JB003492.
- Wood, B. J. (1995), The effect of H_2O on the 410-kilometer seismic discontinuity, *Science*, *268*, 74–76.
- Wood, B. J., A. Pawley, and D. R. Frost (1996), Developments in high-pressure, high-temperature research and the study of the Earth's deep interior, *Philos. Trans. Math. Phys. Eng. Sci.*, *354*, 1495–1551.
- Zhao, D., J. Lei, T. Inoue, A. Yamada, and S. S. Gao (2006), Deep structure and origin of the Baikal rift zone, *Earth Planet. Sci. Lett.*, *243*, 681–691.
- Zorin, Y. A., V. M. Kozhevnikov, M. R. Novoselova, and E. K. Turutanov (1989), Thickness of the lithosphere beneath the Baikal rift zone and adjacent regions, *Tectonophysics*, *168*, 327–337.
- Zorin, Y. A., V. V. Mordvinova, G. L. Kosarev, E. K. Turutanov, B. G. Belichenkoa, and S. S. Gao (2002), Low seismic velocity layers in the Earth's crust of eastern Siberia (Russia) and Mongolia, Receiver function data and geological implication, *Tectonophysics*, *359*, 307–327.

S. S. Gao and K. H. Liu, Department of Geological Sciences and Engineering, University of Missouri-Rolla, MO 65401, USA. (sgao@umr.edu; liukh@umr.edu)